3.5.9

Recent progress in the chopper spectrometer 4SEASONS at J-PARC

R Kajimoto[1], M Nakamura[1], Y Inamura[1], K Kamazawa[2], K Ikeuchi[2], K Iida[2], M Ishikado[2], K Nakajima[1], S Ohira-Kawamura[1], T Nakatani[1], W Kambara[1], H Tanaka[1], Y Yamauchi[1], K Aoyama[1], T Hosoya[1], K Kiriyama[2], K Aizawa[1] and M Arai[1]

[1] Materials and Life Science Division, J-PARC Center, Japan Atomic Energy Agency, Tokai, Ibaraki 319-1195, Japan

[2] Research Center for Neutron Science and Technology, Comprehensive Research Organization for Science and Society (CROSS), Tokai, Ibaraki, 319-1106, Japan

E-mail: ryoichi.kajimoto@j-parc.jp

Abstract. 4SEASONS is a thermal neutron chopper spectrometer operated in the Materials and Life Science Experimental Facility at the Japan Proton Accelerator Research Complex. This instrument has been available to users since 2009, and was declared a public beamline in 2011. On the other hand, the instrument continues to be upgraded by installation of more detectors, development of new choppers, and further attempts to decrease the background scattering. In this article, we review how these progresses have improved the instrument performance and present some results of machine investigations.

1. Introduction

4SEASONS (aka *SIKI* in Japanese) is one of the four chopper spectrometers in the Materials and Life Science Experimental Facility (MLF) at the Japan Proton Accelerator Research Complex (J-PARC). The instrument is designed for measurements of dynamics in the 10^0–10^2 meV energy range with relaxed resolution and high flux [1, 2]. 4SEASONS was originally developed to investigate high critical-temperature (high-T_c) oxide superconductors, and the first inelastic scattering experiment was performed in 2009. Since 2011, 4SEASONS has been classified as a public beamline, and its use has extended to a wider range of studies including chemistry and industry, although studies of superconductors and related materials still comprise the largest proportion of experimental proposals.

A detailed understanding of the instrument's performance is being actively sought, and the instrument continues to be upgraded [3–9]. In this article, we review the recent studies on the performance and the upgrading works of this instrument.

2. Specifications and upgrades of 4SEASONS

2.1. Basic specifications

First, we briefly describe the specifications of the instrument [2]. A schematic of 4SEASONS is presented in Fig. 1. 4SEASONS is installed in the BL01 beamline, whose neutron source is the coupled moderator of supercritical hydrogen [10]. Neutrons are transported through a straight

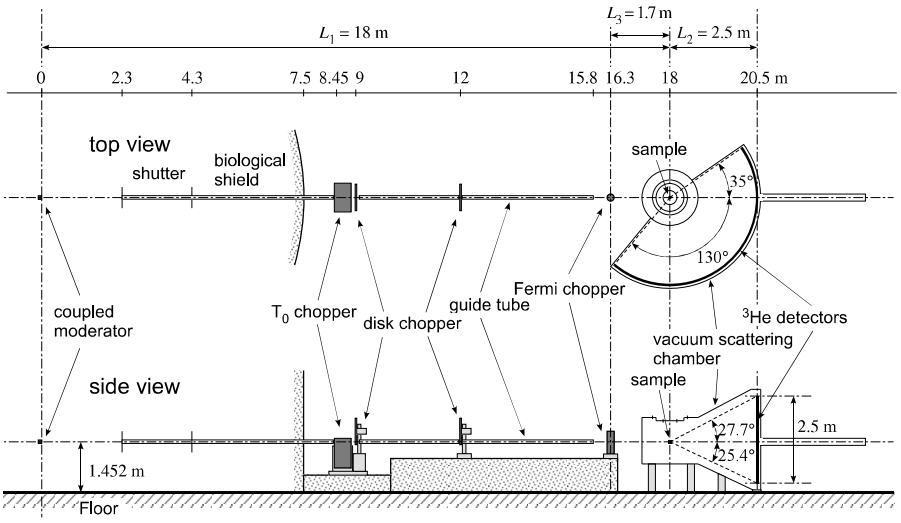

Figure 1. Schematic view of 4SEASONS [2].

neutron guide tube coated with supermirrors, which is installed between 2.3 m downstream from the moderator and 2.2 m upstream from the sample. The cross section of the guide tube gradually decreases with increasing distance from the moderator, focusing neutrons on the sample at $L_1 = 18$ m from the moderator. The m value of the supermirror (ratio of the critical angle to that of the Ni mirror) varies from 3.2 to 4 as a function of the distance [2, 11]. The ∼10–500 meV incident neutrons are monochromated by a fast-rotating Fermi chopper positioned at $L_3 = 1.7$ m upstream from the sample. By taking advantage of the fact that the chopper rotates considerably faster than the repetition rate of the neutron source [12, 13], 4SEASONS can simultaneously perform measurements at multiple incident energies (Multi-E_i measurements) [14]. In addition to the Fermi chopper, there is a T_0 chopper for suppressing fast neutrons and two disk choppers for band definition. The neutrons scattered from the sample are detected over time by the detectors placed $L_2 = 2.5$ m from the sample. The time-of-flight data are acquired by the data acquisition system based on the event-recording [15]. These data are converted to the dynamical structure factor by the software package Utsusemi, which provides a flexible data analysis environment ranging from primitive histogramming of the time-of-flight data to slice-and-cut of single crystal data in the four-dimensional momentum-energy space [3, 16].

2.2. Detectors

4SEASONS is equipped with ^{3}He position-sensitive detectors (PSDs), each having a diameter of 19 mm and length of 2.5 m, cylindrically arranged around the sample (See Fig. 5). The detector bank can be installed with 352 PSD pieces, covering horizontal angles from −35.3° to +130.5° relative to the direct beam. Until recently, however, the angular coverage by the PSDs was only −35.3° to +54.5°. Although such limited range of the scattering angle does not preclude magnetic excitation measurements, it evidently restricts the research targets of the instrument. Unfortunately, the recent ^{3}He crisis prevents us from completely filling the detector bank in the near future. Nevertheless, we are trying to extend the detector coverage as best we can, and PSDs are newly added to the instrument each year. Currently, the maximum horizontal scattering angle is 84.0° (as at the end of fiscal 2014), and is expected to reach 90° in fiscal 2015. The extended detector coverage has already benefited measurements of phonons or atomic vibrations in strongly correlated electron systems and industrial materials.

The PSDs are installed in a vacuum environment; namely, on the posterior wall of the vacuum

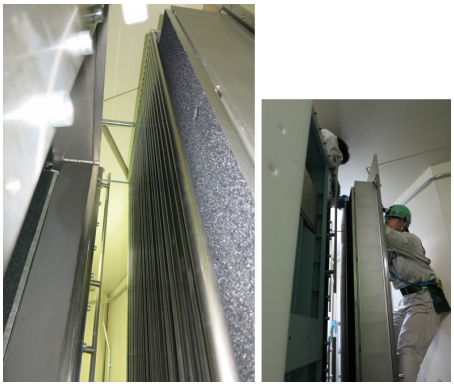

Figure 2. MLF technical staff installing PSDs on one of the detector panels of 4SEASONS.

scattering chamber. This wall, which constitutes the detector bank of 4SEASONS, comprises 11 panels, each of which can hold 32 PSD pieces. Each panel was originally designed to be detached from the vacuum scattering chamber by an overhead crane in the experimental hall. For PSD installation, we had to remove a detector panel from the shielding house using the crane, and lay it upon the floor. However, this proved to be a troublesome task, particularly when frequently installing a small number of PSDs. Recently, we developed a compact jig that slides and fixes one of the detector panels inside the shielding house, which significantly eases the task of installing and uninstalling PSDs. In Fig. 2, MLF staff members use this jig to install PSDs.

2.3. Fermi chopper

The Fermi chopper of 4SEASONS is uniquely characterized by its straight slits. This Fermi chopper allows neutron transmission at every π rotations of the chopper, increasing the number of available E_is in the Multi-E_i measurements [14]. Because straight slits incur greater transmission losses than curved slits, we adopted a wide (sloppy) slits to compensate the extra loss. Each slit is 2 mm wide and 100 mm deep (the width and depth dimensions are dented by w and D, respectively). With this geometry and a rotating frequency f of 600 Hz, the opening time of the Fermi chopper $\Delta t_\mathrm{ch} = w/(2\pi D f)$ equals the pulse width of the moderator Δt_m at $E_\mathrm{i} = 500$ meV [2].

Our straight-slit chopper adopts the same depth dimension as traditional curved-slit choppers ($D = 100$ mm). This dimension is not exactly optimized for the Multi-E_i measurements, because it is too deep to transmit low energy neutrons (energies typically below $\sim$10 meV). Thus, we developed a new Fermi chopper with much shorter slits ($D = 20$ mm). To maintain the spatial divergence w/D of the original chopper, each slit of the new chopper is 0.4 mm wide.

The performance of the new Fermi chopper was estimated in Monte Carlo simulations using the simulation package McStas [17, 18]. Figure 3 compares the calculated energy resolution and neutron flux between the current long-slit chopper and the new short-slit chopper. As the parameter w/D is identical, the energy resolutions of both choppers nearly coincide. On the other hand, the short-slit chopper permits considerably higher neutron flux than the long-slit chopper, particularly at low energies. These results suggest that the new chopper will significantly enhance the performance of 4SEASONS by adopting the new chopper. The new chopper has already been manufactured and delivered to MLF, and will soon be tested with the neutron beam soon.

2.4. Effect of the guide tube on energy resolution

Energy resolution is an essential indicator of instrument performance, and must be correctly estimated to optimize the experimental conditions and improve the chopper design. While

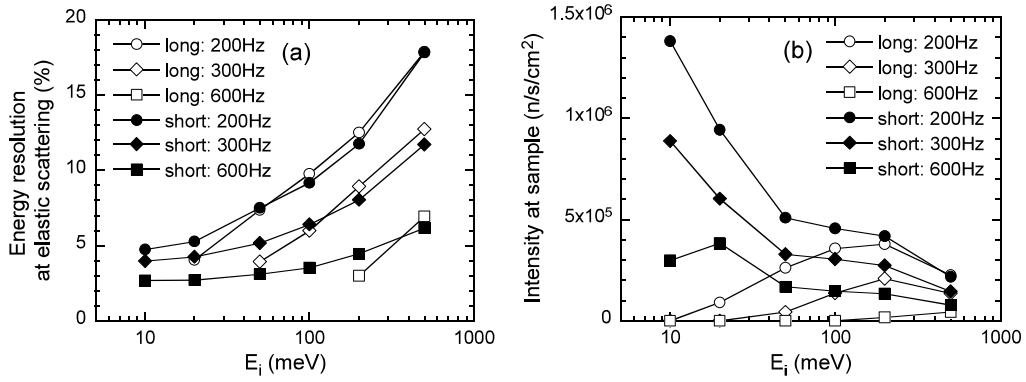

Figure 3. Energy resolution and neutron flux obtained by Monte Carlo simulations of the long-slit chopper (open symbols) and the short-slit chopper (closed symbols) at $f = 200$, 300, and 600 Hz [19]. (a) Energy resolution at the elastic scattering; (b) Neutron flux on a $(2\times2)\,\mathrm{cm}^2$ sample, assuming 1 MW proton beam power.

estimating the energy resolution of a Fermi chopper spectrometer, we must consider the angular divergence of the neutron beam [20]. Beam divergence effects are particularly important if the spectrometer has a neutron guide tube, as does 4SEASONS.

The energy resolution of a chopper spectrometer relative to the incident energy E_i at the energy transfer $\hbar\omega$ is given by the well-known formula [20]

$$\frac{\Delta\hbar\omega}{E_\mathrm{i}} = 2\sqrt{\left\{\frac{\Delta t_\mathrm{ch}}{t_\mathrm{ch}}\left[1+\frac{L_1}{L_2}\left(1-\frac{\hbar\omega}{E_\mathrm{i}}\right)^{\frac{3}{2}}\right]\right\}^2+\left\{\frac{\Delta t_\mathrm{m}}{t_\mathrm{ch}}\left[1+\frac{L_3}{L_2}\left(1-\frac{\hbar\omega}{E_\mathrm{i}}\right)^{\frac{3}{2}}\right]\right\}^2+\left[\frac{\Delta L_2}{L_2}\left(1-\frac{\hbar\omega}{E_\mathrm{i}}\right)\right]^2}, \quad (1)$$

where the path length uncertainty ΔL_2 results from the sample and detector sizes, and t_ch is the neutron time-of-flight from the moderator to the Fermi chopper. For a Fermi chopper with finite depth D, Δt_ch is effectively increased by the angular divergence of the incident neutrons $\Delta\phi_\mathrm{i}$, and becomes [20]

$$\Delta t_\mathrm{ch} = \frac{w}{2\pi D f}p(u). \quad (2)$$

Here $p(u)$ represents the increase in Δt_ch by the angular divergence, and is given by

$$p(u) = \begin{cases} 0 < u < 0.8: & p(u) = 1 + u/4, \\ 0.8 < u < 2: & p(u) = 2 + u - (4u - u^2)^{1/2}, \\ 2 < u: & p(u) = u, \end{cases} \quad (3)$$

where the parameter u is the ratio of $\Delta\phi_\mathrm{i}$ to the angular collimation, defined by the geometry of the slits w/D:

$$u = \Delta\phi_\mathrm{i}/(w/D). \quad (4)$$

In the absence of a guide tube, the $\Delta\phi_\mathrm{i}$ of the chopper spectrometer is constant and determined by the geometry of the instrument [20]. However, in 4SEASONS, neutrons are reflected off the supermirror-coated guide tube; therefore, the $\Delta\phi_\mathrm{i}$ depends on E_i. Specifically, we have

$$\Delta\phi_\mathrm{i} \sim 2\theta_\mathrm{c} \propto E_\mathrm{i}^{-1/2}, \quad (5)$$

where θ_c is the critical reflection angle of the supermirror. Assuming that $\Delta\phi_\mathrm{i}$ is determined by the θ_c of the supermirror at the end of the guide tube, as described in Ref. 5, we can

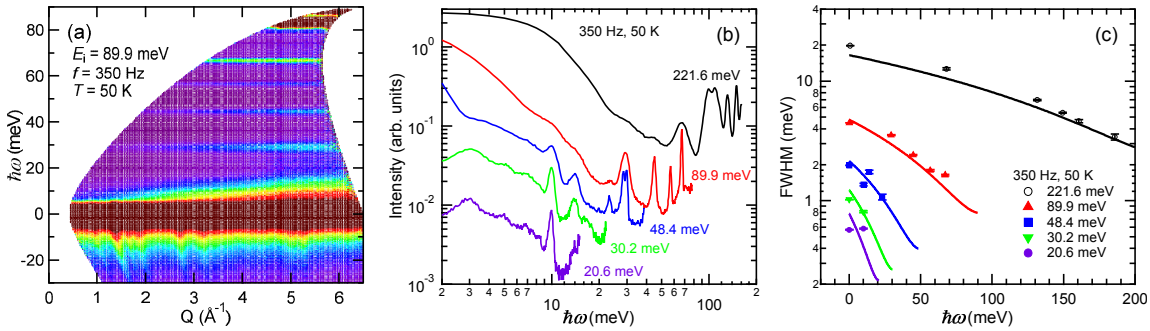

Figure 4. (a) Neutron scattering intensity map of $C_4H_2I_2S$ at $T = 50\,\mathrm{K}$ with $E_\mathrm{i} = 89.9\,\mathrm{meV}$ and $f = 350\,\mathrm{Hz}$. Several non-dispersive modes are clearly observed at $\hbar\omega = 29.3(1)$, 44.8(1), 56.8(1), and 67.0(1) meV, which originate from rotational and vibrational energy modes [21, 22]. (b) Neutron scattering intensities as functions of $\hbar\omega$ at various E_i with $f = 350\,\mathrm{Hz}$, obtained by slicing the neutron scattering intensity maps along the $\hbar\omega$ direction. Data are offset along the vertical axis for clarity. (c) Measured energy resolutions as functions of $\hbar\omega$ at various E_i with $f = 350\,\mathrm{Hz}$, deduced from the FWHMs of the peaks observed in the energy spectra in (b). Solid lines are the energy resolutions for each E_i calculated by Eq. (1), accounting for the angular divergence of the neutron beam [7].

reproduce the observed energy resolution under both elastic and inelastic scattering conditions (see Fig. 4) [2, 7].

The E_i dependence of $\Delta\phi_\mathrm{i}$ significantly influences the optimal energy resolution in a Multi-E_i experiment. If the experimental conditions are optimized, Δt_ch will be comparable to Δt_m in Eq. (1). Δt_m decreases as E_i increases, becoming proportional to $E_\mathrm{i}^{-1/2}$ in the slowing-down region of the moderator ($E_\mathrm{i} \gtrsim 20\,\mathrm{meV}$). Therefore, we cannot optimize the energy resolution at all E_i's in the Multi-E_i measurement, if Δt_ch is independent of E_i, as naively expected for a Fermi chopper rotating at a fixed speed. However, according to Eqs. (2)–(5), Δt_ch and Δt_m are both proportional to $E_\mathrm{i}^{-1/2}$ when w/D is considerably smaller than $\Delta\phi_\mathrm{i}$. Therefore, the energy resolution can be optimized at most of the E_i's by appropriately choosing the rotating frequency of the chopper [5]. On the basis of these considerations, we are developing a new Fermi chopper that optimizes the energy resolution over a wide range of E_i in the Multi-E_i measurements [5, 23, 24].

3. Background scattering problems

3.1. Vanes in the vacuum scattering chamber

As stated in § 2.2, the detectors of 4SEASONS are housed on the detector bank in the vacuum scattering chamber, which constitutes the posterior wall of the chamber. Recently, the gaps between the neighboring detector panels were installed with vertical vanes made of B_4C resin [Fig. 5(a)]. Located parallel to the scattered beam path, these vanes prevent cross-talk of neutrons between the detectors in the chamber. Each vane is 20 mm thick and 530 mm long, where the length is oriented along the beam path. These vane dimensions do not create shadows on the detectors.

To evaluate the effect of the vanes on the background scattering, we measured the inelastic scattering of a test sample that produces weak magnetic excitation signals. Figures 6(a) and 6(b) show the inelastic scattering intensities of a single crystal of $La_{1.92}Sr_{0.18}CuO_4$ at $\sim$5 K before and after vane installation. The data are cross-cut at $\hbar\omega = 125 \pm 15\,\mathrm{meV}$ and presented on the (H, K) plane in the reciprocal lattice. As the (H, K) plane was arranged perpendicular to the

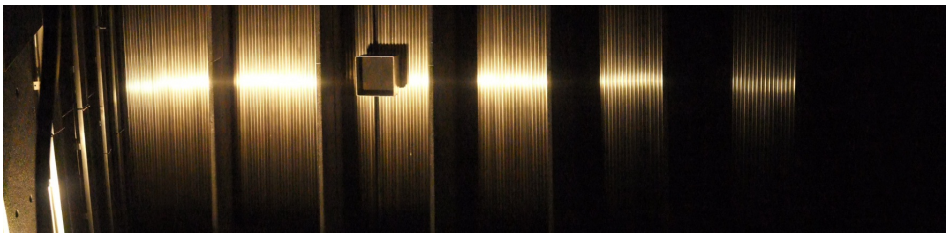

Figure 5. ^{3}He detector tubes and B_4C resin absorbing vanes, installed inside the vacuum scattering chamber of 4SEASONS [4]. The square block is the beam stop, also made of B_4C resin.

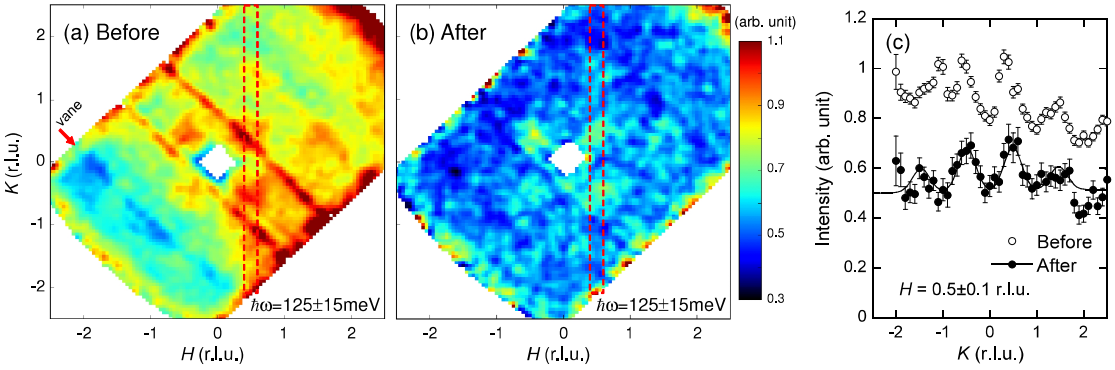

Figure 6. (a) and (b) Intensity maps of the inelastic scattering spectra, measured from a single crystal of $La_{0.82}Sr_{0.18}CuO_4$ at $\sim$5 K with $E_i = 204$ meV before and after the installation of the vanes, respectively [4]. The data are cross-cut at $\hbar\omega = 125 \pm 15$ meV and projected onto the (H, K) plane. The power of the proton beam and the measurement time of the data are 220 kW and 23 h, respectively, in (a), and 120 kW and 8 h, respectively, in (b). The difference in the utilized neutron fluxes is normalized by the proton beam currents. (c) Slices of the data in (a) (open symbols) and (b) (closed symbols) at $H = 0.5 \pm 0.1$. The sliced regions are enclosed by red dotted lines in (a) and (b). Solid line in (c) fits the closed symbols to four Gaussians multiplied by the magnetic form factor for Cu $3d_{x^2-y^2}$ [25].

incident beam, the observed data reflect the geometry of the detector bank. When measuring the data in Fig. 6(a), we had already installed one B_4C vane in a gap between two detector panels; the position of this vane is indicated by the arrow in Fig. 6(a). Although magnetic excitation signals are visible at $(\pm 0.5, \pm 0.5)$ in Fig. 6(a), the entire detector bank (except for the area to the left of the vane) is severely contaminated by the high background. Furthermore, several streaks appear at the positions corresponding to the gaps between the detector panels. These streaks are attributed to neutrons that were scattered by the gaps and subsequently hit the adjacent detectors. In contrast, the vane installation considerably reduces the background over the entire detector bank, and the unwanted streaks completely vanish.

The data in Figs. 6(a) and 6(b) were sliced along the K direction at $H = 0.5 \pm 0.1$, and the slices are presented in Fig. 6(c). The vane installation reduced the background intensity by approximately 40% [cf. closed and open symbols in Fig. 6(c)]. Although the background intensity was not diminished by the vane installation, they should now reflect the intrinsic background introduced by the multi-phonons in the large (96 g) sample. Because of difference in beam power and measurement time, the neutron flux of the data in Fig. 6(b) [and the closed symbols in Fig. 6(c)] is approximately 1/6th that of the data in Fig. 6(a) [and the open symbols

Figure 7. MLF technical staff installing the radial collimator on 4SEASONS.

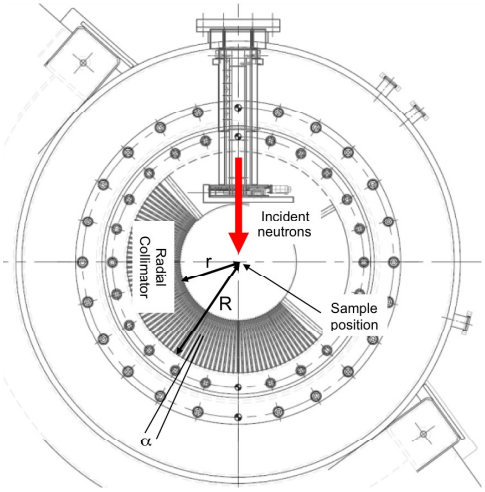

Figure 8. Schematic of a part of the 4SEASONS vacuum scattering chamber installed with the radial collimator. r, R, and α indicate the inner radius, outer radius, and angular separation of the collimator blades, respectively [9].

in Fig. 6(c)]. This reduced neutron flux worsens the statistics of the former data. Nevertheless, the signal-to-noise ratio is sufficiently improved to reveal clear peaks at $K = \pm 0.5$ in Fig. 6(c). Even weaker peaks, whose intensities are reduced by the Q (momentum transfer) dependence of the magnetic form factor, are observable at $K = \pm 1.5$. On the other hand, in the absence of the vanes, the data are contaminated by the high background and the streaks observed in Fig. 6(a), yielding an incorrect excitation profile [see open symbols in Fig. 6(c)].

3.2. Radial collimator

To minimize scattering from the sample environment such as the cryostat or sample can, we have developed a radial collimator [9], an assembly of vertical absorbing blades that radially encloses the sample (Fig. 7). Each blade is an aluminum plate of thickness 100 μm coated on both surfaces with a 25 μm-thick cadmium plating (i.e. the total thickness is 150 μm). By choosing cadmium as the absorbing material, we ensure that the blade contains no hydrogenous materials, and is therefore free of neutron scattering by hydrogen atoms [9]. Figure 8 illustrates the top view of the vacuum scattering chamber of 4SEASONS installed with the radial collimator. The radial collimator is attached to the 800 mm flange of the vacuum scattering chamber, and provides an aperture of the 400 mm flange used by the standard sample environmental devices of MLF. The collimator comprises 72 vertical blades covering a horizontal angular range of -45° to $+135^\circ$. The inner radius r and outer radius R of the collimator are 210 mm and 400 mm, respectively. The angular separation α between the blades is 2.5°. From these dimensions, the diameter of the visible sample d [26] is estimated as $\alpha \cdot rR/(R-r) = 19.3$ mm.

To evaluate the performance of the radial collimator, we compared the elastic neutron scattering profiles in the presence and absence of the collimator. Figure 9 plots the elastic scattering profiles of an 8.5-mm-diameter rod of vitreous silica (v-SiO_2) inserted in a top-loading cryostat. The inner wall of the cryostat is an aluminum cylinder with a 100 mm diameter. In the absence of the radial collimator, the aluminum wall gives rise to strong peaks at certain Q positions (indicated by arrows in Fig. 9). Broad peaks from the non-crystalline SiO_2 are also observed. With the radial collimator installed, the aluminum peaks are significantly

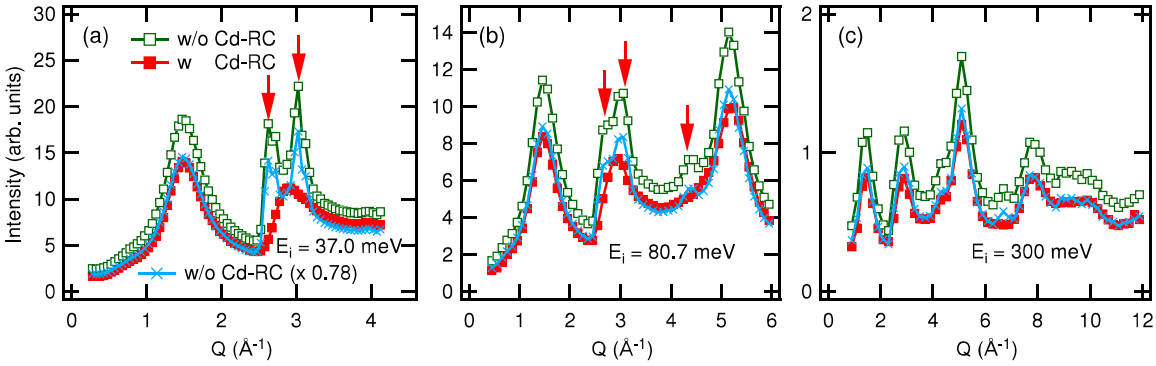

Figure 9. Q dependences of elastic structure factor for v-SiO_2, measured with (solid squares) and without (open squares) the radial collimator with (a) $E_i = 37.0$ meV, (b) 80.7 meV, and (c) 300 meV. Crosses show the intensity of the data without the radial collimator multiplied by 0.78.

attenuated, demonstrating the effectiveness of the radial collimator in suppressing scattering from the sample environment. On the other hand, the radial collimator reduces the intensity of data to approximately 78% that of data collected without the collimator. Given that the size of the sample (8.5 mm) is considerably less than the visible sample size ($d = 19.3$ mm), this transmission is too low . We speculate that intensity might be lost by slight distortion of the cadmium blades. Although this problem is ongoing, the radial collimator has been already used in several measurements. It proved particularly useful in phonon measurements, where the target inelastic scattering signals are often superimposed by aluminum phonons.

3.3. Delayed neutron background

Another major cause of background in instruments such as 4SEASONS, which utilize straight beamlines at spallation neutron sources, is high-energy neutrons that reach the secondary spectrometer directly from the source. Most of these high-energy neutrons are produced when the proton beam hits the neutron target at the time-of-flight $t \equiv 0$ (T_0), and are detected shortly afterward. Such high-energy neutrons are usually suppressed by a T_0 chopper with a thick metal blade [27]. 4SEASONS is equipped with a T_0 chopper with a 300-mm-thick Inconel hammer, which successfully suppresses this class of high-energy neutrons [2, 28]. However, we recently revealed another type of background caused by very fast neutrons that are continuously emitted from the source and transported along the beamline [8]. Although these neutrons are influenced by the Fermi chopper, their ultra-high energies cannot be suppressed by the Fermi chopper. Consequently, the background at the detector oscillates synchronously with the rotational period of the Fermi chopper (see dashed lines in the time-distance plot of Fig. 10). This background is likely sourced by delayed neutrons produced through the β^- decay of nuclides included in the spallation products in the mercury target of MLF [29].

Figure 11 shows a typical time spectrum of the delayed-neutron background. Under the conditions of these data, the incident neutrons that would reach the detector at $t \gtrsim 22\,000\,\mu$s are discriminated by the band choppers, and are further impeded by the long slits of the Fermi chopper. Therefore, no elastic-scattering peak appears in this time region. However, a finite and constant intensity exists [indicated by the dashed line in Fig. 11(a)]. This intensity sharply decreases at $t \sim 40\,000\,\mu$s, when the beamline is blocked by the hammer of the T_0 chopper rotating at 25 Hz. Closer inspection of the time spectrum reveals a temporal oscillation of the background [Fig. 11(b)], which can be decomposed into two oscillations; one with sharp strong peaks [dashed lines in Fig. 11(b)], the other with broader and weaker peaks [dash-dotted lines in Fig. 11(b)]. The sharper and broader peaks coincide with the times of opening the Fermi

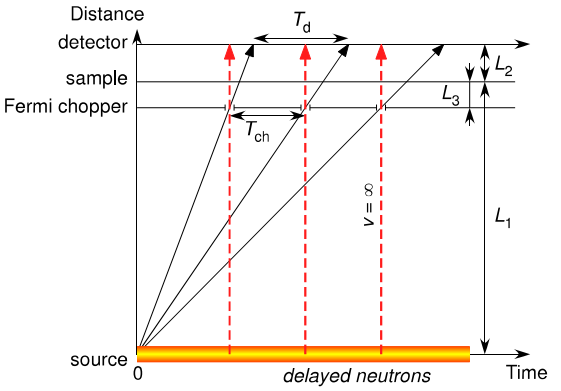

Figure 10. Time-distance diagram of chopper spectrometer [8]. Solid and dashed lines indicate elastic scattering and delayed neutrons, respectively, that pass through the Fermi-chopper opening, which has a period of T_{ch}. Note that T_{ch} is different from the period of the elastic scattering at the detector T_d.

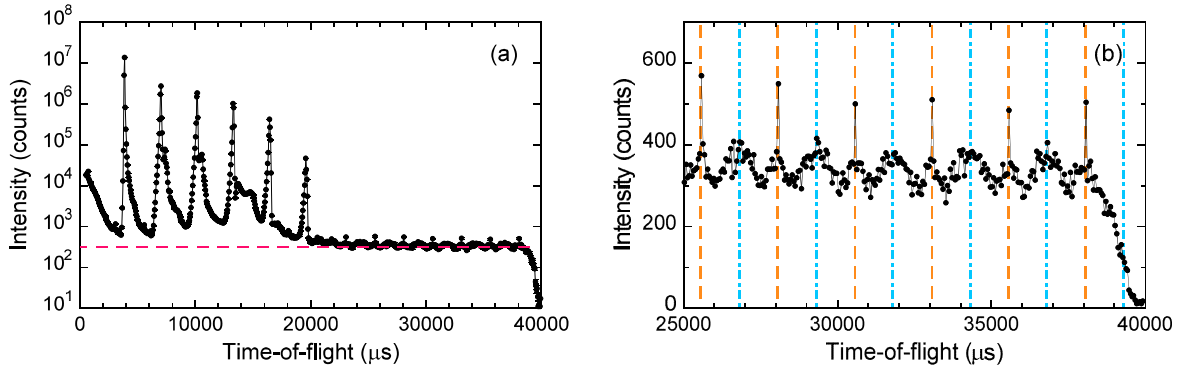

Figure 11. (a) Time spectrum of a single crystal of $La_2CoO_{4.24}$ measured at 6 K for 1.5 d at a proton-beam power of 290 kW [8]. The sharp peaks represent elastic scattering of neutrons with incident energies (in order of increasing time) $E_i = 149$, 45.1, 21.4, 12.5, 8.2, and 5.8 meV. The tails on each elastic-scattering peak manifest from inelastic scattering from the sample. The dashed line indicates the background discussed in the text. (b) Magnified view of panel (a) in the range $20\,000\,\mu s \leq t \leq 40\,000\,\mu s$. Dashed and dash-dotted lines indicate the times of opening the Fermi chopper and rotating it by $\pi/2$, respectively.

chopper and rotating it by $\pi/2$, respectively.

A similar oscillating background was observed by a chopper spectrometer at the ISIS facility of the Rutherford Appleton Laboratory, when the facility used uranium as the neutron target [30]. In this case, the oscillating background originated from delayed neutrons continuously emitted from the fissionable target material. Our observations indicate that, even in facilities using non-fissionable targets, an inelastic-scattering instrument should be carefully designed to offset the delayed neutron effects.

4. Summary

We have reviewed recent progress in the upgrade and performance evaluation studies of the chopper spectrometer 4SEASONS. The increased detector coverage, development of a new Fermi chopper, and successful suppression of background scattering should significantly improve the instrument's performance. To further develop the instrument components such as the Fermi chopper, we require a deeper understanding of the basic performance of the instrument, such as its energy resolution. On the other hand, the recently recognized problem of delayed neutron background might constrain the performance, and requires drastic countermeasures.

Acknowledgments
We thank S. Ji, J. Suzuki, and M. Harada for valuable discussions. We also thank M. Fujita for providing the single crystal of $La_{1.82}Sr_{0.18}CuO_4$ and for valuable discussions. We greatly acknowledge technical support by M. Sawabe, A. Kamiya, K. Inoue, T. Futagami, M. Kobayashi, A. Kishi, and K. Satou. Experiments on 4SEASONS were performed under the approvals of J-PARC and CROSS (proposal nos. 2012B0125, 2012I0001, 2012I0101, 2013I0001, and 2013I0101). The construction of 4SEASONS was supported by KAKENHI (no. 17001001).

References

[1] Kajimoto R *et al.* 2007 *J. Neutron Res.* **15** 5
[2] Kajimoto R *et al.* 2011 *J. Phys. Soc. Jpn.* **80** SB025
[3] Inamura Y, Nakatani T, Suzuki J and Otomo T 2013 *J. Phys. Soc. Jpn.* **82** SA031
[4] Kajimoto R *et al.* 2013 *J. Phys. Soc. Jpn.* **82** SA032
[5] Ikeuchi K, Nakamura M, Kajimoto R and Arai M 2013 *J. Phys. Soc. Jpn.* **82** SA038
[6] Kajimoto R, Nakamura M, Nakajima K and Fujita M 2013 *Nucl. Instrum. Methods Phys. Res.* A **729** 365
[7] Iida K, Ikeuchi K, Ishikado M, Suzuki J, Kajimoto R, Nakamura M, Inamura Y and Arai M 2014 *JPS Conf. Proc.* **1** 014016
[8] Kajimoto R, Nakamura M, Inamura Y, Kamazawa K, Ikeuchi K, Iida K, Ishikado M, Nakajima K, Harada M and Arai M *JPS Conf. Proc.* to be published
[9] Nakamura M *et al. JPS Conf. Proc.* to be published
[10] Maekawa F *et al.* 2010 *Nucl. Instrum. Methods Phys. Res.* A **620** 159
[11] Kajimoto R, Nakajima K, Nakamura M, Soyama K, Yokoo T, Oikawa K and Arai M 2009 *Nucl. Instrum. Methods Phys. Res.* A **600** 185
[12] Mezei F 1997 *J. Neutron Res.* **6** 3
[13] Mezei F, Russina M and Schorr S 2000 *Physica* B **276-278** 128
[14] Nakamura M, Kajimoto R, Inamura Y, Mizuno F, Fujita M, Yokoo T and Arai M 2009 *J. Phys. Soc. Jpn.* **78** 093002
[15] Nakatani T *et al.* 2009 *Proc. 12th Int. Conf. on Accelerator and Large Experimental Physics Control Systems* (Kobe) p 676
[16] Inamura Y, Nakajima K, Kajimoto R, Nakatani T, Arai M, Otomo T, Suzuki J, So J Y and Park J G 2010 *Proc. the 19th Meeting on Int. Collaboration of Advanced Neutron Sources* (Grindelwald) IP117
[17] Lefmann K and Nielsen K 1999 *Neutron News* **10** 20
[18] Willendrup P, Farhi E and Lefmann K 2004 *Physica B* **350** 735
[19] Nakamura M and Kajimoto R 2014 *JPS Conf. Proc.* **1** 014018
[20] Windsor C G 1981 *Pulsed Neutron Scattering* (London: Taylor & Francis Ltd.)
[21] Granroth G E, Kolesnikov A I, Sherline T E, Clancy J P, Ross K A, Ruff J P C, Gaulin B D and Nagler S E 2010 *J. Phys.: Conf. Ser.* **251** 012058
[22] Abernathy D L, Stone M B, Loguillo M J, Lucas M S, Delaire O, Tang X, Lin J Y Y and Fultz B 2012 *Rev. Sci. Instrum* **83** 015114
[23] Nakamura M *et al.* 2014 *Nucl. Instrum. Methods Phys. Res.* A **737** 142
[24] Nakamura M *et al.* 2015 *Proc. the 21nd Meeting on Int. Collaboration of Advanced Neutron Sources* (Mito) this issue

[25] Shamoto S, Sato M, Tranquada J M, Sternlieb B J and Shirane G 1993 *Phys. Rev.* B **48** 13817

[26] Copley J R D and Cook J C 1994 *Nucl. Instrum. Methods Phys. Res.* A **345** 313

[27] Jones T J L, Davidson I, Boland B C, Bowden Z A and Taylor A D 1987 *Proc. the 9th Meeting on Int. Collaboration of Advanced Neutron Sources* (Villingen) p 529

[28] Kajimoto R *et al.* 2010 *Proc. the 19th Meeting on Int. Collaboration of Advanced Neutron Sources* (Grindelwald) IP122

[29] Harada M private communication

[30] Arai M, Taylor A D, Bennington S M, Bowden Z A, Osborn R, Kohgi M, Ohoyama K and Nakane T 1991 *Proc. the 11th Meeting on Int. Collaboration of Advanced Neutron Sources* (Tsukuba) p 644